Information Sciences 575 (2021) 231–247

Contents lists available at ScienceDirect

Information Sciences

journal homepage: www.elsevier.com/locate/ins

First step towards parameters estimation of image operator chain

Xin Liao [a,*], Zihang Huang [a], Lin Peng [a], Tong Qiao [b]

[a] College of Computer Science and Electronic Engineering, Hunan University, Changsha 410082, China
[b] School of Cyberspace, Hangzhou Dianzi University, Hangzhou 310000, China

ARTICLE INFO

Article history:
Received 7 January 2021
Received in revised form 28 May 2021
Accepted 14 June 2021
Available online 17 June 2021

Keywords:
Image forensics
Operator chains
Parameters estimation

ABSTRACT

Many effective techniques have recently been proposed to estimate the parameters of specific tampering operations. Most of them consider the situation in which an image is tampered with by only a single operation. However, in reality, multiple operations are used to falsify an image. Because the tampering traces of previous operations may be weakened or eliminated by later operations, it is difficult for the prior algorithms, each of which was developed for a single operation, to detect all tampering operations. In this paper, we propose a new method for estimating the parameters of operations in different manipulation chains. A framework is presented to investigate the correlation between multiple operations, which divides the degree of correlation into uncoupled and coupled operations. Then, two cases of certain operator chains with different degrees of correlation are adopted to reveal the assessment framework. Under this framework, we design well-directed features to estimate the parameters for each operator chain. Finally, the experimental results demonstrate the effectiveness of the proposed framework.

1. Introduction

Digital images have become ubiquitous in our daily lives. With the rapid development of image editing software, such as Photoshop and GIMP, images can be easily manipulated. In reality, some people can manipulate images for malicious purposes to propagate misinformation. To solve this problem, blind image forensics has become a major research focus.

In recent years, many state-of-the-art forensic techniques have been proposed to detect the specific type of tampering operations, such as copy-move [1–4], splicing [5,6], median filtering [7–9], contrast enhancement [10] and resizing [11,12]. These methods are inapplicable to images with multiple manipulation operations. Therefore, novel detection methods have been designed to identify one specific operation in a processing chain. Bianchi et al. [13] detected the resizing operation in a tampering chain between two JPEG compressions. In this study [14], the contrast enhancement was successfully detected in the middle of a tampering chain between two JPEG compressions.

However, these methods only focus on identifying a specific operation. Given that multiple operations with different operation topologies are always used to tamper images, many methods have been proposed to detect operator chains. The concept of operator chain forensics was first proposed in [15], where the authors theoretically analyzed the possibility of using single-operation tampering forensic algorithms to detect the image manipulation chain. In [16], the zero–height

* Corresponding author.
E-mail address: xinliao@hnu.edu.cn (X. Liao).

https://doi.org/10.1016/j.ins.2021.06.045
0020-0255/

gaps and prediction residuals were involved in detecting the contrast enhancement and scaling, respectively. Furthermore, conditional fingerprints are presented to distinguish the order of these two operations. Based on the non-subsampled contourlet transform, Liu et al. [17] proposed a detection algorithm to determine the order of image blurring and sharpening. In our previous study [18], the sudden gaps and zeros in the histogram and a new adaptive window cutoff function were used to detect the order of contrast enhancement and resizing. In [19], the new symmetry-based PSNR and fourth-order energy fitting curve features were proposed to detect the order of upsampling and median filtering. Gao et al. [20] proposed an efficient information theoretical framework to detect a specific tampering operation in multiple operator chains. In [21], a two-stream convolutional neural network (CNN) architecture for detecting image operator chains was presented.

In addition to identifying the specific operation, some methods have been investigated to estimate the parameters of tampering operations [22–28]. For example, the authors in [22] proposed an energy-based feature called the normalized energy density to estimate the parameters of the resampling. The method was based on variations in energy within the frequency domain. Inspired by this, Zhu et al. [23] adopted a new method called learning-to-rank to automatically estimate the scaling factor. In [24], the authors considered the case of detecting high-quality parameters and nearly identical JPEG image recompression. Based on the Benford-Fourier analysis in the DCT domain and the block convergence analysis in the spatial domain, the authors developed a multipurpose JPEG parameter estimator. Liu et al. [25] found that shifted JPEG block artifacts can produce periodic peaks, which reduce the accuracy in estimating the downscaling factors. To address this problem, an extremum interval histogram of the difference-image and spectral methods was designed to improve the estimation performance. Similarly, by using the mean square error sequence of the DCT coefficient histogram, the authors in [26] estimated the parameters of the first quantization step in double-compressed images. Nandita et al. [27] analyzed the histogram of JPEG images to estimate the parameters of JPEG compression. In [28], the Gamma correction parameters of the contrast enhancement were estimated using image zero histogram features.

However, to the best of our knowledge, no studies have estimated the parameters of the operator chains. Existing studies have only focused on exploring the parameters of a specific operation. When these methods are applied to estimate the parameters of the operator chains, the performance significantly degrades. This is mainly because distinct combinations of tampering operations produce confusing processing effects in the operator chains. The digital features designed for estimating the parameters of specific operations are weakened or even eliminated. Therefore, when detecting one specific operator chain, we not only need to find compatible features that can correctly reveal the changes in the operation parameters, but also investigate whether there exists any correlation between the operations to be estimated.

The initial idea of modeling the correlation between multiple operations based on our framework was proposed in [29], which explores and investigates the parameter estimation strategy in manipulation chains more thoroughly and systematically. In addition, a well-directed method designed for detecting two cases of certain operator chains was proposed and verified experimentally. Specifically, we propose a novel method to estimate the parameters of multiple tampered images by analyzing the correlation degree of multiple operations. First, we exploit the inherent connections among image pixels to investigate the correlation of multiple tampering operations. According to the effects of operation topologies and operation parameters on tampered images, we divide the correlation of operations into uncoupled and coupled operations. To validate the effectiveness of the proposed framework, two operator chains with different degrees of correlation are adopted as examples. Contrast enhancement and median filtering are verified to be uncoupled by exploring the impact of their order on the images. We then prove that resizing and median filtering are coupled from the perspective of the influence of their parameters. For each operator chain, we design well-directed features to estimate the parameters. In particular, we use image histogram and energy density features to estimate the parameters of the contrast enhancement and median filtering. The energy density feature of the difference-image is adopted to detect the factors of resizing and median filtering. The results obtained show significant detection performance for the parameter estimation of the image operator chain.

The remainder of this paper is organized as follows. In Section 2, we introduce the degree of correlation between multiple operations and provide the corresponding discriminant criterion. In Section 3, two cases of specific operator chains are used to demonstrate the proposed method. Section 4 presents the normalized energy density of the difference-image and the image histogram feature. In Section 5, we demonstrate the effectiveness of the proposed method by estimating the parameters of the operator chains with different degrees of correlation. Section 6 provides a corresponding discussion of the results. Finally, some concluding remarks are presented in Section 7.

2. Correlation of tampering operations in operator chains

Various operations are used in the process of image manipulation, and some operations make image pixels a combination of their neighbors. This type of operation introduces periodic correlations into an image [12]. Therefore, different operations will influence each other more or less, which may decrease the accuracy of the parameter estimation. To estimate the parameters more accurately, from the perspective of operation topologies, we further analyze the correlation between distinct operations and divide them into coupled and uncoupled operations. It is relatively easy to estimate the parameters for a combination of uncoupled operations because of the small mutual influence between them. For the combination of coupled operations, owing to their strong correlation, we need to design the targeted parameter estimation features.

First, in terms of operation topologies, the n different operations contained in a tampering chain are denoted as $O = (o_1, o_2, \ldots, o_n)$. $S = (S_1, S_2, \ldots, S_{Num|S|})$ is the set of operator chains generated by combining these operations in any order.

Here, $Num|S| = A_n^n$ denotes the number of different operator chains. We use I_{S_i} to denote a tampered image that experiences a specific operator chain S_i. Based on the relation of the generated images, we propose the first constraint of the discriminant definition. Assuming that the operations in an operator chain are uncoupled, the tampered image should satisfy the following condition:

Definition 1. Assuming the operations in an operator chain are uncoupled, the tampered image should satisfy the following condition

$$I_{S_1} = I_{S_2} = \cdots = I_{S_{Num|S|}} \tag{1}$$

This definition indicates that exchanging the order of multiple operations will not produce any difference in the final generated image, and the above operations do not cover each other. If the tampering operations in an operator chain satisfy Eq. (1), we can define little correlation between these operations. The correlation of this operator chain can be identified as uncoupled. For example, for tampering operations A and B, they are uncoupled if they satisfy Definition 1. Changing their order (A-B or B-A) to tamper the same image will not produce any difference. This indicates that when we use A to tamper with an image and then apply operation B, the tampering traces left by A will not be affected. Therefore, traditional forensic features are effective.

We construct a detection feature $f_{o_i}(\cdot)$ to represent the specific statistical characteristics for detecting operation o_i, and different parameters of o_i can be easily distinguished by $f_{o_i}(\cdot)$. Because changing the order of these operations will not change the final tampered image, the detection results obtained by an selected detection feature $f_{o_i}(\cdot)$ are the same:

$$f_{o_i}(I_{S_1}) = f_{o_i}(I_{S_2}) = \cdots = f_{o_i}(I_{S_{Num|S|}}) \tag{2}$$

Based on the above equation, we can estimate the parameter of each operation in an operator chain respectively and ignore their orders.

In the process of parameter estimation, the main step is to extract the forensic features of the tampering images. Different parameters of operations produce differences in the results of specific forensic features. However, for one operator chain, the correlation between operations may weaken the above differences and make it difficult to distinguish. Thus, to discriminate different operation parameters, we further explore the effect of the later applied operations on the forensic features of the prior operations. We adopt $dist(\cdot)$, which denotes the Euclidean distance to reflect the difference in multidimensional values. Let $\bigcup \theta_i$ denotes the parameters of operation o_i such as

$$\bigcup \theta_i = \left\{ \theta_i^1, \theta_i^2, \ldots, \theta_i^k, \ldots, \theta_i^n \right\} \tag{3}$$

where θ_i^1 is the smallest parameter of operation o_i and θ_i^n is the largest one. For a specific operator chain S_j, it can be expressed as

$$S_j(\theta_1^k, \theta_2^k, \ldots, \theta_n^k), \theta_i^k \in \bigcup \theta_i \tag{4}$$

where $S_j(\theta_i^k)$ represents the specific tampering operator chain S_j including operation o_i with the parameter θ_i^k and other operations.

According to the influence of the correlation between operations on digital features, the second definition is given:

Definition 2. Assuming the operations in an operator chain are coupled, the result of detection feature $f_{o_i}(\cdot)$ will be affected by other operations, i.e.,

$$dist(f_{o_i}(I_{\theta_i^k}), f_{o_i}(I_{\theta_i^{\bar{k}}})) - dist(f_{o_i}(I_{S_j(\theta_i^k)}), f_{o_i}(I_{S_j(\theta_i^{\bar{k}})})) > \varepsilon \tag{5}$$

where θ_i^k and $\theta_i^{\bar{k}}$ are different parameters for the same operation o_i, and ε indicates a threshold value. If the difference value is within this range, it means that the detection results of different parameters of o_i are not significantly affected by other operations. The above formula explains the criteria for judging whether the operation is coupled. More specifically, if operation o_i is coupled with the other operations, the feature $f_{o_i}(\cdot)$ will be affected by other operations in an operator chain, which will further reduce the difference between different operating parameters in the detection results. For example, for some monotonic features, if the tampering traces of a specific operation value are weakened by later operations, the detection feature may be mixed with other parameters, which will reduce the detection accuracy. Therefore, if the tampering operations in an operator chain satisfy Eq. (5), we can define these operations as coupled; otherwise, they are uncoupled.

The framework for distinguishing the correlations between multiple operations is shown in Fig. 1. To distinguish whether the operations are uncoupled, we first use tampering manipulations with different orders to tamper the same raw images and obtain the corresponding tampered image. We then compare the pixel values in the same coordinates as these images. When an image experiences several tampering operations that satisfy Definition 1 (i.e., the pixel values are the same), we can identify that they are uncoupled. Otherwise, from the perspective of the operation parameters, we tamper with the images using a single operation and operator chain, and then use Definition 2 to further distinguish whether they are coupled.

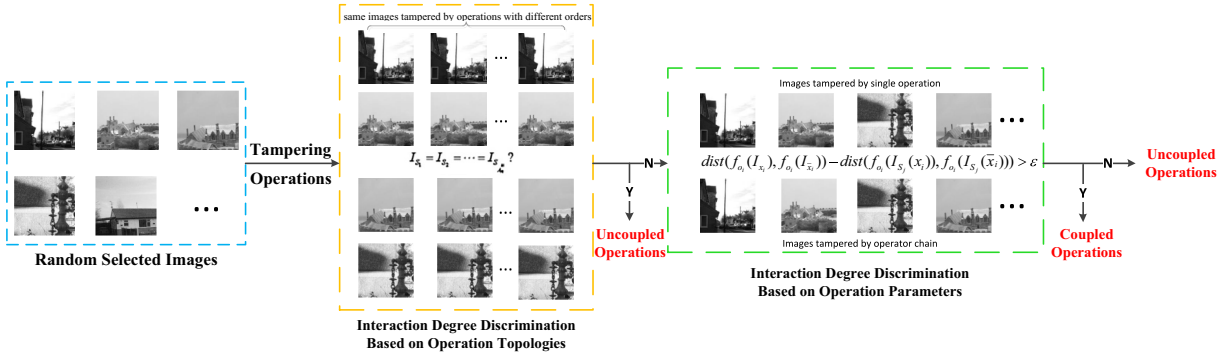

Fig. 1. The framework of distinguishing the correlation degree between multiple operations.

If the operations are coupled, we construct the digital features of each operation to estimate their parameters. Moreover, because of the difference in the degree of correlation introduced by a distinct operation sequence, the order should be considered when estimating the parameters. If the operations are uncoupled, the parameters can be estimated separately by adopting most existing methods used for detecting single operations.

3. Correlation between multiple operations: uncoupled and coupled

In this section, we use specific tampering operations to clarify the framework for distinguishing the degree of correlation between multiple operations. In the present study, we consider an image tampered with by two different operations. Furthermore, according to Definitions 1 and 2, we determine whether the operations are coupled by the difference in the correlation between tampering operations. By exploring the influence of the operation parameters on the digital features, we identify the median filtering and resizing following Definition 2, which are coupled.

3.1. Analysis of uncoupled operations

As shown in Section 2, for a given image I, we assume that it has experienced several specific operations with any order denoted as $I_{S_1}, I_{S_2}, \ldots, I_{S_n}$. If there is no difference among the generated images, we can conclude that they are independent of each other. In a real application, contrast enhancement and median filtering are always adopted to improve the visual effect of the image. In particular, median filtering is a nonlinear smoothing operation that converts the current pixel into the median value of its correlation window. A contrast enhancement applies a nondecreasing nonlinear calculation to each pixel value. In this section, these two operations are used to demonstrate the details of Definition 1. The image underwent median filtering, and the contrast enhancement is denoted as I_{S_1}. In addition, I_{S_2} represents the image tampered with by the reverse operation order.

Firstly, we describe an original $n \times n$ image I experienced median filtering then contrast enhancement:

$$I = \begin{bmatrix} p(1,1) & p(1,2) & \cdots & p(1,n) \\ p(2,1) & p(2,2) & \cdots & p(2,n) \\ \vdots & \vdots & \ddots & \vdots \\ p(n,1) & p(n,2) & \cdots & p(n,n) \end{bmatrix} \tag{6}$$

where $p(i,j)$ is the pixel corresponding to the coordinate (i,j). Then, we assume that the window size of median filtering is $(2l+1) \times (2l+1)$. The correlative window $W(i,j)$ of the $p(i,j)$ is

$$W(i,j) = \begin{bmatrix} p(i-l,j-l) & \cdots & p(i-l,j+l) \\ \vdots & \ddots & \vdots \\ p(i+l,j-l) & \cdots & p(i+l,j+l) \end{bmatrix} \tag{7}$$

Especially, we use $m(p(i,j))$ to represent the median value of a pixel's correlative window. After median filtering, the tampered image T is given as

$$T = \begin{bmatrix} m(p(1,1)) & m(p(1,1)) & \cdots & m(p(1,n)) \\ m(p(2,1)) & m(p(2,2)) & \cdots & m(p(2,n)) \\ \vdots & \vdots & \ddots & \vdots \\ m(p(n,1)) & m(p(n,2)) & \cdots & m(p(n,n)) \end{bmatrix} \tag{8}$$

Contrast enhancement applies a nonlinear mapping to the pixel values of an image. It mainly consists of the process of Gamma correction

$$G(p) = [(p + 0.5)/256]^{1/\gamma} \times 256 - 0.5 \tag{9}$$

where p denotes the pixel value and γ is the factor of Gamma correction. According to the above equations, we can finally obtain the pixel $p_1(i,j)$ in the tampered image I_{S_1} that experienced median filtering then contrast enhancement

$$p_1(i,j) = G(m(p(i,j))) \tag{10}$$

Next, we consider the reverse order. From the discussion above, we can easily acquire the pixel $q(i,j)$ of the image after contrast enhancement

$$q(i,j) = G(p(i,j)) \tag{11}$$

And the pixel $p_2(i,j)$ in the final generated image I_{S_2} which experienced contrast enhancement then median filtering is

$$p_2(i,j) = m(q(i,j)) = m(G(p(i,j))) \tag{12}$$

Finally, the first derivative of Eq. (9) is

$$G'(p) = \frac{\partial G(p)}{\partial p} = \frac{\frac{(p+0.5)^{\frac{(1-\gamma)}{\gamma}}}{256}}{\gamma} > 0 \tag{13}$$

The ∂ here is the process of getting the first derivative. Because of $G'(p) > 0$, the function $G(p)$ is monotonically increasing. Gamma correction does not change the numerical relationship of pixels in an image, and after contrast enhancement, the pixels value is directly related to the monotone function. Specifically, for a 3×3 image I, $p(i,j)$ represents the pixel values of it. We assume that the pixel values in this image are in a certain order(i.e. $p(2,2)$ is the median value). According to formula 8, $(m(I) = m(p(2,2)) = p(2,2))$ is established. Here, $m(\cdot)$ is the process of finding the median value. If $m(I) = p(2,2)$, we can obtain $m(G(I)) = G(p(2,2))$ after contrast enhancement. The median value after Gamma correction keeps the same as before. Similarly, we applied median filtering then contrast enhancement on the same pixel window. After median filtering, the median value of the fixed-size window is $p(2,2)$. And the final generated pixel value after contrast enhancement is $G(p(2,2))$. According to the above process, the values of pixels in tampered images I_{S_1} and I_{S_2} are equal, $p_1(i,j) = p_2(i,j)$. Therefore, $I_{S_1} = I_{S_2}$.

Fig. 2 shows the difference in the tampered images experiencing the contrast enhancement and median filtering with different orders. The window size of median filtering is 3×3, and the factor of the contrast enhancement is 1.2. Figs. 2(b) and (c) are images tampered with by adopting the contrast enhancement and median filtering with distinct sequences. To distinguish whether these two images are the same and satisfy Definition 1, we calculate the difference in the pixel values in their same coordinates. The all-black image in Fig. 2(c) is the calculation, and there is no difference between these two images. This indicates that exchanging the order of contrast enhancement and median filtering will not change the final

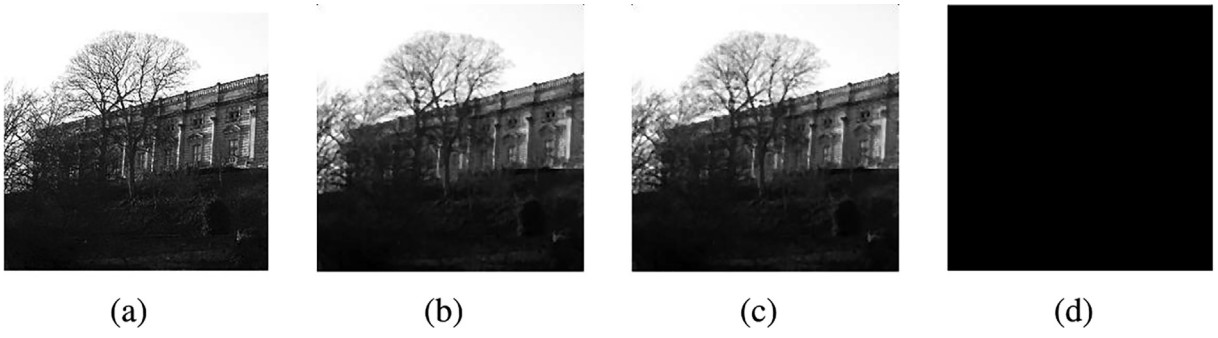

Fig. 2. The difference of tampered images. (a) is the original image, (b) is the image experienced contrast enhancement then median filtering, (c) is the image experienced median filtering then contrast enhancement, (d) is the difference between (b) and (c).

image. Thus, we can conclude that contrast enhancement and median filtering satisfy Definition 1, and that they are uncoupled.

3.2. Analysis of coupled operations

If changing the order of tampering operations will influence the final images, we need to further analyze whether the operations are coupled. As mentioned before, we explore the influence of the operation parameters on the digital features. Similarly, median filtering and resizing are used to clarify Definition 2 in this section. Here, I_{S_1} denotes that the tampered image experiences median filtering followed by resizing, and I_{S_2} denotes the reverse order. Image resizing involves an interpolation process that introduces new pixels around the original pixels. In the interpolation process of this operation, the inserted pixels are related to their surrounding pixels. First, we describe an original $n \times n$ image that undergoes median filtering and resizing. Here, we use bilinear interpolation as an example. The vertical direction is similar to the horizontal direction in the resizing process. To simplify the description process, we only discuss bilinear interpolation in the horizontal direction with a ratio of greater than 1. From Eq. (8), we know the pixel values in an image after applying median filtering:

$$M(i,j) = m(p(i,j)) \tag{14}$$

where $p(i,j)$ is the pixel of the original image. It is known that, bilinear involves interpolation in the horizontal and vertical direction. In order to get the value of the target newly generated pixel, we first adopt interpolation in the horizontal direction and get the pixel matrix I_{S_h}:

$$I_{S_h} = \begin{bmatrix} M_1(1,1) & N_1(1,1) & \cdots & M_1(1,2) & \cdots \\ M_1(2,1) & N_1(2,1) & \cdots & M_1(2,2) & \cdots \\ \vdots & \vdots & \ddots & \vdots & \vdots \\ M_1(n,1) & N_1(n,1) & \cdots & M_1(n,2) & \cdots \end{bmatrix} \tag{15}$$

where $M_1(i,j)$ is the pixel calculated by Eq. (14) and $N_1(i,j)$ is the newly generated pixel after interpolation in the horizontal direction. For bilinear interpolation, these pixels are related to their adjacent original pixels. Next, we discuss the first column of them

$$\begin{cases} N_1(i,1) = \alpha M_1(i,1) + \beta M_1(i,2) \\ N_1(i+1,1) = \alpha M_1(i+1,1) + \beta M_1(i+1,2) \end{cases} \tag{16}$$

where α and β are the weights related to resizing factors. Then we can adopt the generated pixels and calculate interpolation in the vertical direction to obtain the final interpolation result $N_1(i',1)$

$$N_1'(i,1) = \gamma N_1(i,1) + \delta N_1(i+1,1) \tag{17}$$

where γ and δ are the weights related to resizing factors. And the final generated image I_{S_1} is

$$I_{S_1} = \begin{bmatrix} M_1(1,1) & N_1(1,1) & \cdots & M_1(1,2) & \cdots \\ \cdots & N_1'(1,1) & \cdots & \cdots & \cdots \\ \vdots & \vdots & \ddots & \vdots & \vdots \\ M_1(2,1) & N_1(2,1) & \cdots & M_1(2,2) & \cdots \\ \vdots & \vdots & \ddots & \vdots & \vdots \\ M_1(n,1) & N_1(n,1) & \cdots & M_1(n,2) & \cdots \end{bmatrix} \tag{18}$$

Similarly, if modifying the order of operations, resizing the original image first, the first column of newly generated pixels in the horizontal direction is defined as

$$\begin{cases} R(i,1) = \alpha p(i,1) + \beta p(i,2) \\ R(i+1,1) = \alpha p(i+1,1) + \beta p(i+1,2) \end{cases} \tag{19}$$

And the result $R(i',1)$ of the interpolation process is

$$R'(i,1) = \gamma R(i,1) + \delta R(i+1,2) = \gamma(\alpha p(i,1) + \beta p(i,2)) + \delta(\alpha p(i+1,1) + \beta p(i+1,2)) \tag{20}$$

After median filtering, we can find the $R(i',1)$ is changed to

$$N_2'(i,1) = m(R'(i,1)) \tag{21}$$

The final tampered image I_{S_2} is

$$I_{S_2} = \begin{bmatrix} M_2(1,1) & N_2(1,1) & \cdots & M_2(1,2) & \cdots \\ \cdots & N_2'(1,1) & \cdots & \cdots & \cdots \\ \vdots & \vdots & \ddots & \vdots & \vdots \\ M_2(2,1) & N_2(2,1) & \cdots & M_2(2,2) & \cdots \\ \vdots & \vdots & \ddots & \vdots & \vdots \\ M_2(n,1) & N_2(n,1) & \cdots & M_2(n,2) & \cdots \end{bmatrix} \tag{22}$$

where $M_2(i,j) = m(p(i,j))$. Because the pixels existed in a fixed window of median filtering is changed after resizing, the results of $M_1(i,j)$ and $M_2(i,j)$ might be different. If median filtering and resizing are uncoupled, changing the order of them would not influence the tampered image. Further, the first column of newly generated pixels should be the same, i.e.,

$$N_1'(i,1) = N_2'(i,1) \tag{23}$$

To compare $N_1'(i,1)$ and $N_2'(i,1)$ more clearly, according to Eqs. (14) and (16), the newly generated pixel $N'(i,1)$ can be expressed as

$$N_1'(i,1) = \gamma(\alpha m(p(i,1)) + \beta m(p(i,2))) + \delta(\alpha m(p(i+1,1)) + \beta m(p(i+1,2))) \tag{24}$$

In a similar way, Eq. (21) could be converted into

$$N_2'(i,1) = m(R'(i,1)) = m(\gamma(\alpha p(i,1) + \beta p(i,2)) + \delta(\alpha p(i+1,1) + \beta p(i+1,2))) \tag{25}$$

As mentioned above, interpolation process will introduce new pixels in the fixed window of median filtering and $m(\cdot)$ is a nonlinear operation. Therefore, it hardly holds true that $N_1'(i,1)$ and $N_2'(i,1)$ could be equal by comparing between Eqs. (24) and (25) (i.e. $I_{S_1} \neq I_{S_2}$).

Fig. 3 is the image histograms of an original image and the tampered images experienced resizing and median filtering with different orders. The window size of median filtering is 3×3 and the factor of resizing is 1.5. We can conclude that changing the order of the two operations would influence the final tampered image. Therefore, median filtering and resizing do not satisfy Definition 1. According to our framework, we need to further analyze their digital features.

Based on Definition 2, if an operation's digital trace would be much affected by others, we can define that they are coupled. In this part, the influence of median filtering on resizing detection is used to demonstrate our method. Given most parameters estimation features designed for resizing, we choose the most representative image energy features.

Firstly, on the basis of Parseval's equation, the energy E of a $n \times n$ image can be expressed as

$$E = \sum_{x=1}^{n}\sum_{y=1}^{n} p(i,j)^2 = \sum_{u=-\omega}^{\omega}\sum_{v=-\omega}^{\omega} |P(u,v)|^2 \tag{26}$$

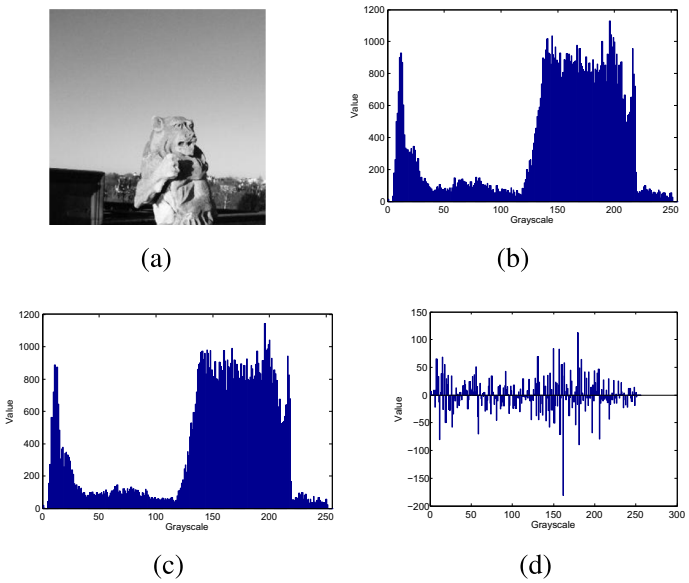

Fig. 3. Histogram of an tampered image. (a) is the original image, (b) is the histogram of the image that experienced resizing before median filtering, (c) is the histogram of the image that experienced median filtering before resizing, (d) is the difference of (b) and (c).

where ω is the cutoff frequency of the image, $p(i,j)$ is the pixel value and $P(u,v)$ is the frequency spectrum.

Let $E_{\omega_c}(\cdot)$ denotes the energy of the high-frequency part of a resized image, while $E_{\omega}(\cdot)$ is the energy of the entire resized image. After applying resizing with parameter r, the ratio of $E_{\omega_c}(r)$ and $E_{\omega}(r)$ is

$$\frac{E_{\omega_c}(r)}{E_{\omega}(r)} = \frac{\sum_{u=-\omega_c}^{\omega_c}\sum_{v=-\omega_c}^{\omega_c}|P_r(u,v)|^2}{\sum_{u=-\omega}^{\omega}\sum_{v=-\omega}^{\omega}|P_r(u,v)|^2} = a \tag{27}$$

where ω_c is the selected cutoff frequency, $P_r(u,v)$ is the frequency spectrum of a resized image with parameter r and $a \in (0,1)$. Repeatedly, we apply resizing on the same image with a smaller parameter $\bar{r}$. Based on the energy based method, the ratio of the energy between the high-frequency part and the whole image would be reduced. It can be expressed as

$$\frac{E_{\omega_c}(\bar{r})}{E_{\omega}(\bar{r})} = \frac{\sum_{u=-\omega_c}^{\omega_c}\sum_{v=-\omega_c}^{\omega_c}|P_{\bar{r}}(u,v)|^2}{\sum_{u=-\omega}^{\omega}\sum_{v=-\omega}^{\omega}|P_{\bar{r}}(u,v)|^2} = k \times a \tag{28}$$

where $k < 1$. The difference between the results of detecting operation parameter r and $\bar{r}$ is

$$dist(\tfrac{E_{\omega_c}(r)}{E_{\omega}(r)}, \tfrac{E_{\omega_c}(\bar{r})}{E_{\omega}(\bar{r})}) = \tfrac{E_{\omega_c}(r)}{E_{\omega}(r)} - \tfrac{E_{\omega_c}(\bar{r})}{E_{\omega}(\bar{r})} = (1-k) \times a \tag{29}$$

where $\frac{E_{\omega_c}(r)}{E_{\omega}(r)}$ and $\frac{E_{\omega_c}(\bar{r})}{E_{\omega}(\bar{r})}$ corresponds to $f_{o_i}(I_{\theta_i^k})$ and $f_{o_i}(I_{\theta_i^{\bar{k}}})$ in Eq. (5), respectively.

It is generally known that median filtering is a nonlinear digital filter technology, the value of the center pixel is determined by sorting the pixels' gray level in the selected window which is related to the parameters. Median filtering can remove isolated grey values and image noise that would generate smoother images. Because image frequency represents the degree of image gray level change, the high-frequency part of the smoother image would be reduced accordingly. Therefore, if we further apply median filtering on the above images, the result of Eq. (29) would become

$$dist(\frac{E'_{\omega_c}(r)}{E'_{\omega}(r)}, \frac{E'_{\omega_c}(\bar{r})}{E'_{\omega}(\bar{r})}) = \lambda_r \times a - \lambda_{\bar{r}} \times ka = a \times (\lambda_r - \lambda_{\bar{r}} \times k) \tag{30}$$

where $\lambda_r < 1, \lambda_{\bar{r}} < 1$. $\frac{E'_{\omega_c}(r)}{E'_{\omega}(r)}$ and $\frac{E'_{\omega_c}(\bar{r})}{E'_{\omega}(\bar{r})}$ represents $f_{o_i}(I_{S_j(\theta_i^k)})$ and $f_{o_i}(I_{S_j(\theta_i^{\bar{k}})})$ in Eq. (5). In our method, we need to calculate the difference between Eqs. (29) and (30). The result is

$$dist(\tfrac{E_{\omega_c}(r)}{E_{\omega}(r)}, \tfrac{E_{\omega_c}(\bar{r})}{E_{\omega}(\bar{r})}) - dist(\tfrac{E'_{\omega_c}(r)}{E'_{\omega}(r)}, \tfrac{E'_{\omega_c}(\bar{r})}{E'_{\omega}(\bar{r})}) = a \times ((1-\lambda_r) - (1-\lambda_{\bar{r}}) \times k) \tag{31}$$

where $k < 1, a > 0$ and the values of λ_r and $\lambda_{\bar{r}}$ are close in most scenarios. Therefore, $dist(\frac{E_{\omega_c}(r)}{E_{\omega}(r)}, \frac{E_{\omega_c}(\bar{r})}{E_{\omega}(\bar{r})}) - dist(\frac{E'_{\omega_c}(r)}{E'_{\omega}(r)}, \frac{E'_{\omega_c}(\bar{r})}{E'_{\omega}(\bar{r})}) > \varepsilon$. The feature designed for distinguishing different resizing parameters is much affected by median filtering. The difference between the detection results of distinct parameters is reduced. Therefore, Definition 2 is satisfied.

As an example, we adopt the forensic feature based on the energy in image frequency domain [22] denoted as $f_o(\cdot)$ to detect resized images. We first apply resizing to tamper original images, respectively. Here, $I_{\theta_i^k}$ denotes the image experiences resizing with parameter $\theta_i^k < 1$ and the image experiences resizing with parameter $\theta_i^{\bar{k}} > 1$ is represented as $I_{\theta_i^{\bar{k}}}$. Then, resizing with different parameters and median filtering are applied to the same images. They are denoted as $I_{S_j(\theta_i^k)}$ and $I_{S_j(\theta_i^{\bar{k}})}$, respectively. Fig. 4 shows median filtering obviously weakens the digital features for estimating different resizing parameters, i.e., $dist(f_{o_i}(I_{\theta_i^k}), f_{o_i}(I_{\theta_i^{\bar{k}}})) - dist(f_{o_i}(I_{S_j(\theta_i^k)}), f_{o_i}(I_{S_j(\theta_i^{\bar{k}})})) > \varepsilon$.

Overall, from the perspective of detection features, resizing and median filtering are satisfy Definition 2, and they are coupled.

4. Estimation features of specific operator chains

Based on the correlations and characteristics of different operations, we propose well-directed estimation strategies and features for detecting operator chains. If the operations are coupled, we construct the digital features of each operation to estimate their parameters. Owing to the difference in the correlation introduced by distinct operation sequences, the order of multiple operations should be considered. If two operations are uncoupled, the parameters can be estimated separately by adopting most existing methods used to detect single operations. Meanwhile, during the process of estimating the parameters, if the order of the operations is changed, the detection results are consistent. In this section, we discuss several supervised algorithms to estimate the parameters of the two cases mentioned above: (1) contrast enhancement and median filtering and (2) median filtering and resizing.

4.1. Contrast enhancement and median filtering

As mentioned in Section 2, median filtering is a nonlinear smoothing operation, and contrast enhancement is a technique that includes non-decreasing nonlinear mapping, which are uncoupled operations. In this operator chain, exchanging their

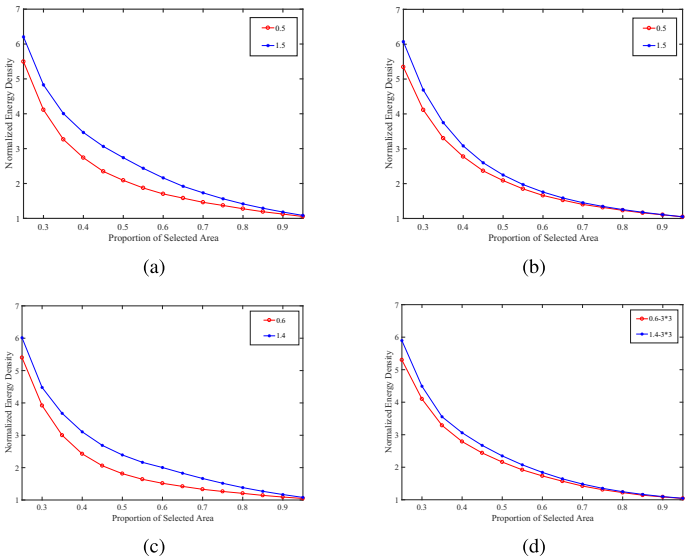

Fig. 4. Averaged normalized energy density of 100 tampered images. (a) is the images applied resizing with parameter 0.5. (b) is the images applied resizing then median filtering with window size 5×5. (c) represents the images applied resizing with parameter 0.6. (d) is the images applied resizing then median filtering with window size 3×3.

order does not create any difference in the tampered images. Therefore, we used two different features to estimate their parameters. In our previous study [18], a histogram feature was proposed as a single-operation detection algorithm to detect contrast enhancement.

As an extension, we improve this histogram feature of digital images and then create a 254-dimensional image histogram feature to estimate the parameters of the contrast enhancement, the details of which are as follows.

$$H(i) = \frac{H(i) - H_{mean}}{H_{std}}, i = 1, 2, \cdots, 254 \tag{32}$$

where $H(i)$ is the i-th dimension of the features, H_{std} and H_{mean} denote the standard deviation and mean of the histogram.

As is shown in Fig. 5, we calculate the averaged image histogram feature of 1000 images which applying contrast enhancement with different parameters from BOSS database [30]. Distinct Gamma correction parameters can be easily separated by using our proposed features. The farther the parameter is to 1, the more peaks and valleys appear.

Median filtering is a nonlinear smoothing operation and the pixel value of the corresponding coordinate is the median value of its correlation window. Therefore, it will make the image smoother and influence the frequency domain of tampered images. In this part, we adopt the energy-based feature in [22] to estimate the parameters of median filtering. The feature is

$$E_n(w) = \frac{\sum |\hat{p}(u, v)|^2}{w^2 \sum |p(u, v)|^2} \tag{33}$$

where $w \in (0, 1]$ is the proportion of the selected area in the frequency domain, $\sum \hat{p}(u, v)$ and $\sum p(u, v)$ are the sum of frequency spectrum value of the selected area and the whole image, respectively.

We apply median filtering to 1000 raw images in BOSS database [30] with different window sizes: $3 \times 3, 5 \times 5$ and 7×7, and then calculate their mean normalized energy density. To show the feature in different dimensions clearly, we make logarithmic operation ($log_2(\cdot)$) on the results. As is shown in Fig. 6, we can find that the energy-based feature is effective and the window size of median filtering could be easily distinguished.

4.2. Resizing and median filtering

In Section 2, we prove that there exists a certain correlation between the resizing and median filtering. In particular, median filtering weakens the periodic artifacts introduced by resizing. The manipulation traces of these two operations are covered by each other, and both influence the energy within the frequency domain. Therefore, we improve the normalized energy density method by extending the feature dimensions and highlighting the differences between the different parameters to achieve a parameter estimation. In this section, a difference-image that can highlight the texture details of one image is introduced to enhance the normalized energy density method. The distribution of the difference-image can be accurately expressed through a generalized Gaussian distribution. Based on simplifying the features, the differences in the vertical and

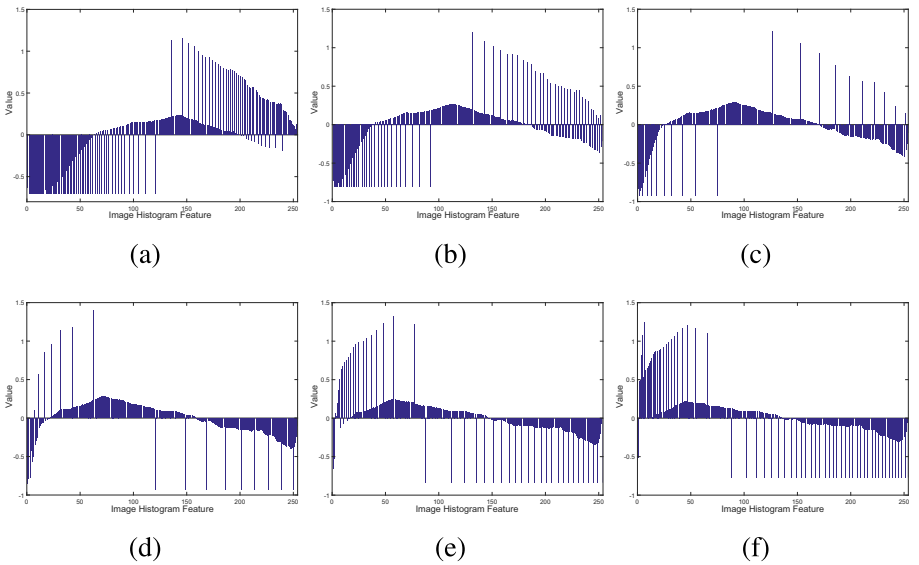

Fig. 5. Averaged image histogram feature of 1000 images after contrast enhancement. The value of Gamma correction is 0.5, 0.7 and 0.9 in (a)–(c), the value of Gamma correction is 1.1, 1.3 and 1.5 in (d)–(f).

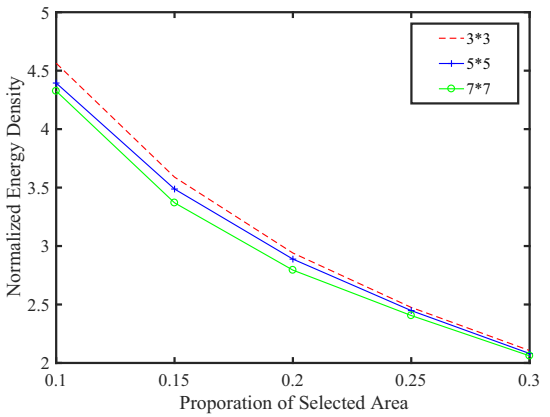

Fig. 6. The normalized energy density curves for different window sizes of median filtering.

horizontal directions are used to extend the dimensions of the features. Here, we first define the difference image of a gray image

$$\begin{cases} p_x(i,j) = p(i+1,j) - p(i,j), i,j = 1,2,\ldots,n-1 \\ p_x(n,j) = p(n,j) \end{cases} \tag{34}$$

where $p_x(i,j)$ is the difference-image of an $n \times n$ gray image in the vertical direction, $p(i,j)$ represents the pixel value in the original image

$$\begin{cases} p_y(i,j) = p(i,j+1) - p(i,j), i,j = 1,2,\ldots,n-1 \\ p_y(i,n) = p(i,n) \end{cases} \tag{35}$$

where $p_y(i,j)$ is the difference-image of an $n \times n$ gray image in the horizontal direction. The pixel value of each column is obtained by subtracting current column from the next. Fig. 7 shows the difference-image of an original image in the vertical and horizontal direction.

Before calculating the normalized energy density, we need to reduce the strong low-frequency components within the spectrum. In our method, the Laplacian filter is adopted to highlight the high-frequency portion of the digital images. It is a two-dimensional discrete approximation of Laplacian operators. Specifically, we use a filter with a kernel K

(a) (b) (c)

Fig. 7. Difference-image. (a) is the original image. (b) is the difference-image in the vertical direction, (c) is the difference-image in the horizontal direction.

$$K = \begin{bmatrix} 0 & -1 & 0 \\ -1 & 4 & -1 \\ 0 & -1 & 0 \end{bmatrix}$$

Then, we use Eq. (33) to compute the normalized energy density. In order to obtain adequate feature dimensions, the normalized energy density with different window sizes is adopted as our forensic features. The window size is in the range [0.1,0.95] with the step of 0.05, the number of different window sizes is $(0.95 - 0.1)/0.05 = 18$. Therefore, we can acquire an 18-dimensional feature from every image including the gray image and the difference-image in two directions.

Fig. 8 shows the mean normalized energy densities of 1000 tampered images. These images experienced resizing then median filtering with different resizing factors and the median filtering window size is 5×5. The normalized energy density features of different operation parameters are distinct. Thus, we could use this energy-based feature in the original image and difference-image to form a multi-dimensional feature, and then estimate the parameters of resizing and median filtering.

5. Experimental results

In this section, the details of image datasets and the setting of our experiments are provided. Meanwhile, we show the detecting performance of our proposed framework by estimating the parameters of two different operator chains: (1) contrast enhancement and median filtering. (2) median filtering and resizing.

5.1. Experimental settings

During the experiments, two different image datasets are used to form the training and test sets. In particular, we use the BOSS database [30], which contains 10,000 raw images as a training set and uses the UCID database [31] as a test set. To obtain sufficient training images, we crop the full-size images from the BOSS database to a size of 256×256 using the horizontal and vertical median lines. Similarly, we crop the images from the UCID database by selecting their 256×256 central parts. Based on the digital features, every color image is converted into a gray image.

We extract image features corresponding to different operation parameters, and diverse features are mapped to distinct categories. In our experiment, specific parameters are estimated by analyzing the results of the trained SVM classifiers. For example, if the parameters of resizing to be estimated range from 0.4 to 1.8, with a step size of 0.2, there will exist eight outputs of the trained SVM classifiers. The estimation result of the classifier is a category label corresponding to a specific parameter. Therefore, we record the result as correct when the estimated label is accurate (i.e., the estimated value is consistent with the true value).

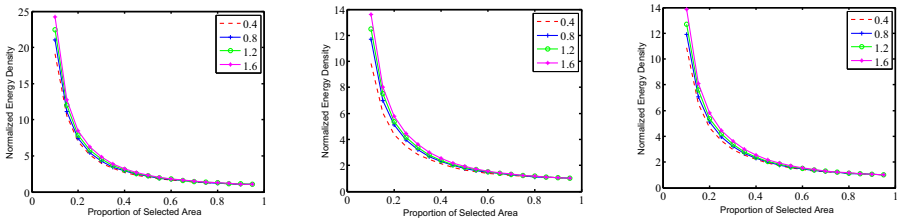

(a) (b) (c)

Fig. 8. Normalized energy densities of a tampered image. (a) is the normalized energy densities of gray image, (b) is the normalized energy densities of difference-image in the vertical direction and (c) is the normalized energy densities of difference-image in the horizontal direction.

The features designed for estimating the parameters of the operator chains are used as input to train multi-class support vector machine (SVM) classifiers with a radial basis function (RBF) kernel. Considering that contrast enhancement and median filtering are uncoupled operations, we estimate their parameters. Therefore, our experiment involves a 3-category problem and an 11-category problem. In our experiment for detecting the median filtering and resizing, 24 output classes exist. The details of the experiment are as follows.

5.2. Performance in parameters estimation of contrast enhancement and median filtering

In Section 3, we proved that contrast enhancement and median filtering are uncoupled operations, and median filtering has little effect on estimating the parameters of a contrast enhancement. Therefore, most detection algorithms that are designed only for contrast enhancement can be used to estimate the correct parameters.

To verify the efficiency of our results, we adopt the 254-D image histogram feature proposed in Section 3 to estimate the parameters of the contrast enhancement in images that only experienced such enhancement, as well as in images that experienced both contrast enhancement and median filtering. The Gamma correction parameter in the contrast enhancement ranges from 0.5 to 1.1 in steps of 0.1, and the window size of the median filtering is 5×5. In this part, the training set contains 1500 images from the BOSS database for each parameter.

According to these experiments, we find the detection accuracy of two operation settings is extremely close, applying median filtering would not decrease the accuracy of detecting contrast enhancement. In conclusion, contrast enhancement and median filtering are uncoupled operations, there exists little correlation between them.

For contrast enhancement and median filtering in an operator chain, we make experimental data sets with 33 different pairs of parameters by combining the factors of these two operations in different order,

- The window size of median filtering includes $3 \times 3, 5 \times 5, 7 \times 7$.
- The parameter of Gamma correction in contrast enhancement ranges from 0.5 to 1.5 in steps of 0.1.

According to our analysis described in Section 3, contrast enhancement and median filtering are uncoupled and satisfy Constraint 1. Therefore, two multiclass classifiers can be used to estimate their factors. More specifically, to estimate the parameters of median filtering, we first modify 1500 raw images from the BOSS database using each median filtering parameter. A contrast enhancement is then applied with a factor of 1.2, which is randomly selected. After the above operations, we obtain 4500 tamper images to form a total training set. Next, the 18-D vector of every image proposed in Section 3 is used as input to train the SVM classifiers, where the polynomial kernel is set as the kernel function. Finally, we select 1000 images from the UCID database to generate a test set containing all combinations of operations. Table 1.

After obtaining the trained classifier to estimate the parameters of the median filtering, the next step is to train a multiple classifier to detect the contrast enhancement. Similarly, we randomly select 1500 raw images from the BOSS database. These images are then tampered with using each parameter of the contrast enhancement, and median filtering is then applied with a window size of 5×5. As a result, we acquire 16500 images as our training set. The proposed 254-D vector of each image is then used as input to train the SVM classifier. The test set is the same as that used in the previous experiment. The experimental results for detecting the chain of median filtering and contrast enhancements are shown in Table 2 and Fig. 9. Here, we use the non-machine learning algorithm proposed in [28] for contrast. In [28], Wang et al. estimated the Gamma correction parameters of a contrast enhancement by applying zero histogram features. Their method estimates the parameters of the contrast enhancement to multiple decimal places. We round off the estimation result and keep one decimal place. As an example, if the actual parameter of the contrast enhancement is 0.8, we record results of between 0.75 and 0.85 as correct. The average detection accuracies of our proposed method and Wang's approach [28] are 87.7% and 81.3%, respectively. When the Gamma correction parameter of the contrast enhancement is less than 0.9 and more than 1.4, Wang's method [28] performs better. By comparison, our method is comparable and more stable when the value of the parameter is more than 0.9, and less than 1.5.

The experimental results verify the availability of the parameter estimation strategy in the proposed framework for uncoupled operations in the operation chain described in Section 2. If the operations are uncoupled, the methods designed for detecting single operations can achieve good results.

5.3. Performance in parameters estimation of median filtering and resizing

In this section, we use our proposed method to detect median filtering and resizing with different operation parameters,

Table 1
Results of our method estimating the parameters of images experienced contrast enhancement and contrast enhancement then median filtering (%).

settings	0.5	0.6	0.7	0.8	0.9	1	1.1	1.2	1.3	1.4	1.5	AVG
CE	95.4	95.6	96	96.6	94.1	98.4	94.9	96.6	98.5	98.4	98.6	96.6
CE-MF	96.1	95.8	96.7	97.3	94.9	96.2	96	97.4	98.9	98.6	98.5	96.9

Table 2
Comparisons between our proposed method and [28] for estimating the parameters of images experienced median filtering and contrast enhancement (%).

parameters	0.5		0.6		0.7		0.8		0.9		1		1.1		1.2		1.3		1.4		1.5	
	Ours	[28]	Ours	[28]	Ours	[28]	Ours	[28]	Ours	[28]	Ours	[28]	Ours	[28]	Ours	[28]	Ours	[28]	Ours	[28]	Ours	[28]
3×3	92.8	94.1	91.2	94.4	90.8	94.6	88.8	93.7	88.0	86.1	86.5	71.0	87.9	43.2	89.0	76.1	90.9	87.3	91.7	91.6	90.7	94.2
5×5	89.3	90.2	87.3	90.7	87.2	90.7	85.2	89.9	84.5	83.9	83.3	64.5	83.6	36.4	85.2	68.2	87.2	81.2	87.6	87.2	86.8	89.9
7×7	90.8	91.5	88.6	92.5	88.5	92.0	86.5	91.4	85.8	85.7	85.0	65.4	84.3	36.5	86.3	65.1	88.4	82.2	88.7	88.7	87.7	91.4

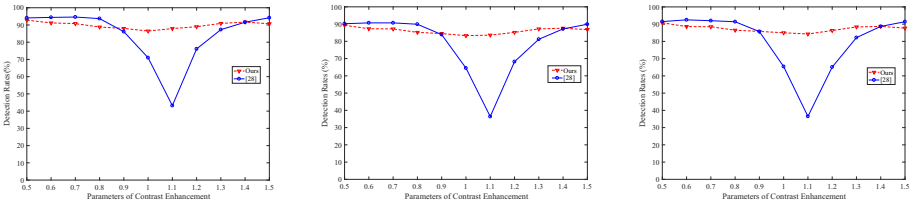

Fig. 9. Detection accuracy of images experience median filtering and contrast enhancement. (a) the parameters of median filtering is 3×3, (b) the parameters of median filtering is 5×5, (c) the parameters of median filtering is 7×7.

- The window size of median filtering includes $3 \times 3, 5 \times 5, 7 \times 7$.
- The parameter of resizing ranges from 0.4 to 1.8 in steps of 0.2.

Because median filtering and resizing are coupled, the influence of different orders on the generated images is different. In this section, we train two multiclass classifiers for different operation sequences. For each operation order, we tampered with 1000 raw images from the BOSS database using each median filtering and resizing parameter. As a result, we create 24,000 tampered images as the training set for a single classifier. Meanwhile, 1000 UCID images are generated with each pair of parameters as a test set.

Table 3 shows the accuracy rates for detecting images tampered by resizing with factors of 0.4 to 1.8, and then median filtering with different window sizes. From this table, it can be observed that our method can effectively estimate the parameters used during the operations. Similarly, our method can correctly estimate the parameters of images tampered with through median filtering and resizing. The detection results are presented in Table 4. As mentioned before, the correlation between different operations will influence the performance of the detectors designed for a single operation, and median filtering and resizing satisfy Constraint 2. Therefore, the performance of our method is comparable to that of the method mentioned in [22] by applying a difference-image.

In reality, the original images are always stored in JPEG format after being tampered with. To verify the robustness of our proposed method, we tamper with 1000 raw images from the BOSS database using different pairs of operation parameters and operation orders. We then apply JPEG compression with a quality factor of 95 to save every image. Finally, we obtain 24,000 JPEG images to train the classifiers. Similarly, for each operation parameter and operation order, we tamper with 1000 images from the UCID database and further compressed these images with quality 95 to form the test set. Tables 5 and 6 present the detecting performance of our method and the method proposed in [22]. In contrast, our method is more effective to estimate the parameters of JPEG images and the average accuracy rates have more than 8% of rising. Fig. 10 is the line chart of average accuracy.

In this experiment, an SVM classifier is adopted to estimate the operation parameters by mapping distinct digital features to different categories. Therefore, the estimated parameters are discrete values. For trained classifiers, specific values can be estimated in the determined interval and step sizes. When a higher detection accuracy is required (e.g., the resizing parameter is 0.55), we can adjust the range of parameters and step size according to the preliminary detection results and the required accuracy. As an example, we can set the parameters to a range of 0.4–0.8, with a step size of 0.05, and train a new classifier. The parameters can then be estimated within a certain range of accuracy.

6. Discussions

In this paper, we propose a framework for estimating the parameters of different manipulation chains. Our work focuses only on the parameter estimation of the operator chain. Thus, the proposed method is based on the assumption that, prior to estimating the parameters of an operation chain using our framework, we already know the types of manipulations that have been applied. We must acknowledge that our method has certain limitations. For a given image, we do not know whether it has been tampered with and what the manipulations are in real life. However, we can complete the judgment

Table 3
Comparisons between our proposed method and [22] for estimating the parameters of images experienced resizing then median filtering (%)

parameters	0.4		0.6		0.8		1		1.2		1.4		1.6		1.8	
	Ours	[22]	Ours	[22]	Ours	[22]	Ours	[22]	Ours	[22]	Ours	[22]	Ours	[22]	Ours	[22]
3×3	91.0	88.0	89.6	76.3	90.6	78.2	84.7	83.6	83.2	76.4	74.8	64.3	91.8	86.6	76.5	67.5
5×5	90.7	87.0	88.1	76.3	90.4	76.9	82.2	71.2	82.2	75.4	75.5	62.1	93.2	89.5	80.8	70.2
7×7	81.2	77.0	90.4	78.0	91.4	83.9	86.3	74.4	84.3	78.2	72.9	64.8	93.6	89.9	73.5	61.8

Table 4
Comparisons of our proposed method and [22] for estimating the parameters of images experienced median filtering then resizing (%)

parameters	0.4		0.6		0.8		1		1.2		1.4		1.6		1.8	
	Ours	[22]	Ours	[22]	Ours	[22]	Ours	[22]	Ours	[22]	Ours	[22]	Ours	[22]	Ours	[22]
3×3	87.2	87.4	90.8	86.2	91.0	87.5	90.7	78.8	89.2	78.2	89.4	77.3	90.2	80.5	91.5	78.7
5×5	84.0	87.0	91.5	85.8	90.7	87.2	88.8	78.0	87.1	76.0	88.5	77.6	91.0	79.2	90.0	80.9
7×7	86.5	82.5	89.0	80.6	91.1	84.5	91.0	79.7	90.2	78.8	90.7	77.6	90.6	80.2	93.7	76.4

Table 5
Comparisons of our proposed method and [22] for estimating the parameters of JPEG images experienced resizing then median filtering (%)

parameters	0.4		0.6		0.8		1		1.2		1.4		1.6		1.8	
	Ours	[22]	Ours	[22]	Ours	[22]	Ours	[22]	Ours	[22]	Ours	[22]	Ours	[22]	Ours	[22]
3×3	93.9	83.0	92.7	78.2	96.2	82.6	83.8	79.1	86.7	82.1	82.2	77.3	91.5	93.3	88.1	89.9
5×5	91.9	83.7	89.3	79.3	91.2	81.5	83.5	76.3	83.1	78.2	72.6	64.2	91.7	86.9	78.0	70.4
7×7	88.1	74.4	89.4	72.8	91.6	79.5	85.2	68.9	87.1	76.5	71.7	60.6	94.6	91.8	77.7	63.0

Table 6
Comparisons of our proposed method and [22] for estimating the parameters of JPEG images experienced median filtering then resizing (%)

parameters	0.4		0.6		0.8		1		1.2		1.4		1.6		1.8	
	Ours	[22]	Ours	[22]	Ours	[22]	Ours	[22]	Ours	[22]	Ours	[22]	Ours	[22]	Ours	[22]
3×3	82.8	81.9	89.5	87.7	94.9	90.7	89.0	82.4	89.9	83.6	86.9	77.7	92.5	86.4	89.9	83.9
5×5	81.9	75.8	89.5	87.0	92.1	88.1	90.4	82.8	87.4	77	86.6	76.9	91.8	81.4	86.9	81.4
7×7	86.5	83.5	91.1	84.0	93.1	84.9	90.6	73.2	88.4	77.6	90.6	78.1	92.7	82.5	87.8	77.9

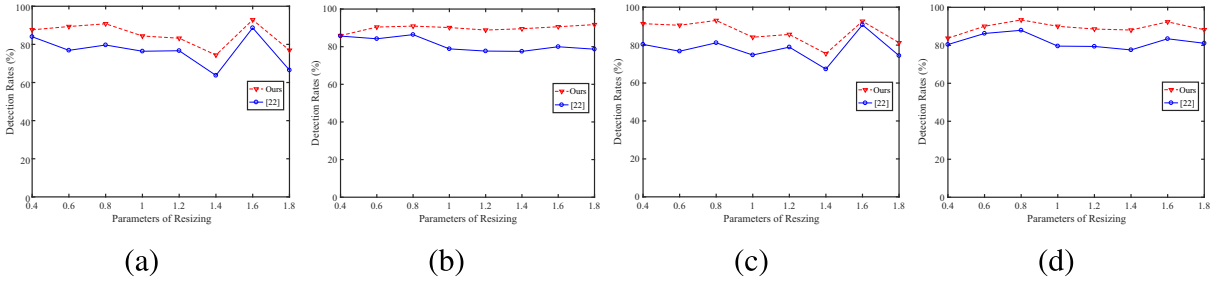

Fig. 10. Averaged detection accuracy of images experienced resizing and median filtering. (a) is raw images experienced resizing then median filtering, (b) is raw images experienced median filtering then resizing, (c) is JPEG images experienced resizing then median filtering, (d) is JPEG images experienced median filtering then resizing.

using universal image forensic methods. The framework therefore plays a significant role in the parameter estimation of different operator chains.

Moreover, we show two cases of certain operator chains, which include three operations: contrast enhancement, median filtering, and resizing. In a realistic scenario, the types of operations in the chain are not limited to those mentioned in our paper, and we can also tamper with images using other operations. However, this work focuses more on the degree of correlation between operations, rather than on the operations themselves. The proposed framework divides such correlation into uncoupled and coupled correlations. Then, based on the correlation, the corresponding detection feature is designed to estimate the parameters of the operation chains. The results of the two cases show that the proposed framework is of importance to the parameter estimation of the operator chains.

Currently, operation parameter estimation based on machine learning algorithms adopts a classification method (e.g., SVM). These methods map different parameters to the corresponding categories to obtain parameter estimation results. Different precision results can be obtained by adjusting the parameter intervals. Compared with regression techniques (e.g., SVR), classification methods do not need to fit the best calculation curves. Therefore, the difficulty of data training is smaller when using the classification methods. Considering the advantages of a higher precision of regression, in the future, we will explore applying regression to detect the operation parameters, focusing on improving the estimation accuracy and reducing the amount of training data requirements.

In our proposed method, we only consider the operation chains that contain two operations as examples to demonstrate the effectiveness of the framework. We have to admit that there could be more than two operations applied to images in

realistic scenes. However, we find almost all of the reference documents in past studies only designed for estimating the parameters of one specific operation, and no work involves the operator chains. Existing methods that target one specific operation may not obtain acceptable performance for a chain. Moreover, as the number of operations increases, the correlation between the operations may change. Therefore, considering that more complex correlations exist between different manipulations, more effective estimation strategies would be designed for such chains.

7. Conclusion

In this paper, a new method is proposed to estimate the operation parameters in different operator chains. The main contributions of this study are summarized as follows:

- To the best of our knowledge, no study has analyzed the parameters of the operator chain. From the perspective of operation topologies, we first propose a framework to further estimate the parameters of the tampering operations in different manipulation chains.
- By investigating the inherent correlation between different tampering operations, we divide the degrees of correlation of the operator chains into two categories: coupled and uncoupled.
- Two cases of certain operator chains with different degrees of correlation are adopted to verify the framework. Moreover, well-directed features are proposed for these cases. The experimental results proved that the proposed method is effective and useful for both original and JPEG images.

In the future, we will continue to extend the number of operations to more than two manipulations. The digital features we proposed will also be modified to improve the accuracy.

CRediT authorship contribution statement

Xin Liao: Conceptualization, Methodology, Formal analysis, Writing - review & editing. **Zihang Huang:** Methodology, Software, Investigation, Writing - original draft. **Lin Peng:** Validation, Data curation. **Tong Qiao:** Validation, Supervision.

Declaration of Competing Interest

The authors declare that they have no known competing financial interests or personal relationships that could have appeared to influence the work reported in this paper.

Acknowledgment

This work is supported by National Natural Science Foundation of China (Grant Nos. 61972142, 61772191, 61702150), Hunan Provincial Natural Science Foundation of China (Grant No. 2020JJ4212), Science and Technology Program of Changsha (Grant No. kq2004021), Key Lab of Information Network Security, Ministry of Public Security (Grant No. C20611).

References

[1] J.C. Lee, C.P. Chang, W.K. Chen, Detection of copy-move image forgery using histogram of orientated gradients, Information Sciences 321 (2015) 250–262.
[2] X. Bi, C.M. Pun, Fast reflective offset-guided searching method for copy-move forgery detection, Information Sciences 418–419 (2017) 531–545.
[3] J. Zhong, C.M. Pun, Dense moment feature index and best match algorithms for video copy-move forgery detection, Information Sciences 537 (2020) 184–202.
[4] J. Zhong, C.M. Pun, Two-pass hashing feature representation and searching method for copy-move forgery detection, Information Sciences 512 (2019) 675–692.
[5] B. Xiao, Y. Wei, X. Bi, et al, Image splicing forgery detection combining coarse to refined convolutional neural network and adaptive clustering, Information Sciences 511 (2020) 172–191.
[6] B. Liu, C.M. Pun, Exposing splicing forgery in realistic scenes using deep fusion network, Information Sciences 526 (2020) 133–150.
[7] X. Kang, M. Stamm, A. Peng, K.J.R. Liu, Robust median filtering forensics using an autoregressive model, IEEE Transactions on Information Forensics and Security 8 (9) (2013) 1456–1468.
[8] A. Peng, S. Luo, H. Zeng, Median filtering forensics using multiple models in residual domain, IEEE Access 7 (2019) 28525–28538.
[9] C. Chen, J. Ni, J. Huang, Blind detection of median filtering in digital images: A difference domain based approach, IEEE Transactions on Image Processing 22 (12) (2013) 4699–4710.
[10] N. Singh, A. Gupta, R. Jain, Global contrast enhancement based image forensics using statistical features, Advances in Electrical and Electronic Engineering 15 (3) (2017) 509–516.
[11] M. Kirchner, R. Bohme, Hiding traces of resampling in digital images, IEEE Transactions on Information Forensics and Security 3 (4) (2008) 582–592.
[12] A. Popescu, H. Farid, Exposing digital forgeries by detecting traces of resampling, IEEE Transactions on Signal Processing 53 (2) (2008) 758–767.
[13] T. Bianchi, A. Piva, Reverse engineering of double JPEG compression in the presence of image resizing, IEEE International Workshop on Information Forensics and Security (2012) 127–132.
[14] P. Ferrara, T. Bianchi, Reverse engineering of double compressed images in the presence of contrast enhancement, IEEE International Workshop on Multimedia Signal Processing (2013) 141–146.
[15] P. Comesaña, Detection information theoretic measures for quantifying the distinguishability between multimedia operator chains, IEEE International Workshop on Information Forensics and Security (2012) 211–216.

[16] M. Stamm, X. Chu, Forensically determining the order of signal processing operations, IEEE International Workshop on Information Forensics and Security (2013) 162–167.
[17] Y. Liu, Y. Zhao, R. Ni, Forensics of image blurring and sharpening history based on NSCT domain, IEEE Signal and Information Processing Association Annual Summit and Conference (2014) 1–4.
[18] Gao S., Liao X., Guo S., Forensic detection for image operation order: resizing and contrast enhancement, International Conference on Security, Privacy and Anonymity in Computation, Communication and Storage, 2017, pp. 570–580..
[19] J. Li, X. Liao, R. Hu, Detectability of the image operation order: upsampling and mean filtering, Asia-Pacific Signal and Information Processing Association Annual Summit and Conference (2018) 1544–1549.
[20] S. Gao, X. Liao, X. Liu, Real-time detecting one specific tampering operation in multiple operator chains, Journal of Real-Time Image Processing 16 (3) (2019) 741–750.
[21] X. Liao, K. Li, X. Zhu, K.J.R. Liu, Robust detection of image operator chain with two-stream convolutional neural network, IEEE Journal of Selected Topics in Signal Processing 14 (5) (2020) 955–968.
[22] X. Feng, I. Cox, G. Doerr, Normalized energy density-based forensic detection of resampled images, IEEE Transactions on Multimedia 14 (2012) 536–545.
[23] N. Zhu, C. Deng, X. Gao, A learning-to-rank approach for image scaling factor estimation, Neurocomputing 204 (2016) 33–40.
[24] Pasquini C., Schöttle P., Böhme R., Forensics of high quality and nearly identical jpeg image recompression, ACM Workshop on Information Hiding and Multimedia Security ACM, 2016, pp. 11-21. .
[25] X. Liu, W. Lu, Q. Zhang, Downscaling factor estimation on pre-JPEG compressed images, IEEE Transactions on Circuits and Systems for Video Technology (2019), https://doi.org/10.1109/TCSVT.2019.2893353.
[26] F. Xue, Z. Ye, W. Lu, H. Liu, MSE period based estimation of first quantization step in double compressed JPEG images, Signal Processing: Image Communication 57 (2017) 76–83.
[27] D. Nandita, O. Manish, Robust first quantization matrix estimation based on filtering of recompression artifacts for non-aligned double compressed JPEG images, Signal Processing: Image Communication 61 (2018) 9–20.
[28] P. Wang, F. Liu, C. Yang, Parameter estimation of image gamma transformation based on zero-value histogram bin locations, Signal Processing: Image Communication 64 (2018) 33–45.
[29] X. Liao, Z. Huang, A framework for parameters estimation of image operator chain, IEEE International Conference on Acoustics, Speech and Signal Processing (2020) 2787–2791.
[30] B. Patrick, T. Filler, T. Pevný, Break our steganographic system: the ins and outs of organizing BOSS, International Workshop on Information Hiding (2011) 59–70.
[31] G. Schaefer, M. Stich, UCID: an uncompressed color image database, Storage Retr. Methods Appl. Multimed 5307 (1) (2004) 472–481.